ADVANCED OPTICAL FIBER COMMUNICATION SYSTEMS

ONR Status Report for the period August 1, 1992 through February 28, 1993

R&T Project Code: 4148130-01

Grant Number: N00014-91-J-1857

Professor Leonid G. Kazovsky, Principal Investigator

Department of Electrical Engineering

Durand 202, MC-4055

Stanford University

Stanford, CA 94305-4055

Our research is focused on theoretical investigations of advanced optical fiber communication systems and can be grouped into three broad areas: WDM networks, coherent analog links, and optical fiber nonlinearities. In the area of WDM networks, we proposed and investigated a novel WDM network architecture (STARNET), a novel combined phase/amplitude modulation format, and a high-speed optics-to-computer interface for STARNET. In the area of coherent analog links, we investigated angle and amplitude modulated systems for linewidth-insensitive analog applications and direct-frequency-modulated subcarrier-multiplexed systems. In the area of fiber nonlinearities, we investigated four-wave mixing, thermally induced parasitic phase modulation, and a new type of soliton.

A detailed summary of our efforts is provided in the following sections. Section 1 describes our efforts in WDM networks. Sections 2 and 3 describe our efforts in coherent analog links and fiber nonlinearities.

1. WDM Networks

PSK/ASK Modulation Format: In the previous ONR Status Report, we reported our proposal of a new broadband network architecture, STARNET, based on a passive star topology. STARNET supports both circuit-switched traffic and packet-switched traffic by creating two logical sub-networks, a 2.488 Gb/s (chosen for compatibility with the SONET standard) per node tunable circuit-switched sub-network and a 100 Mb/s FDDI-compatible, fixed-tuned, packet-switched, ring sub-network, on a single physical star topology.

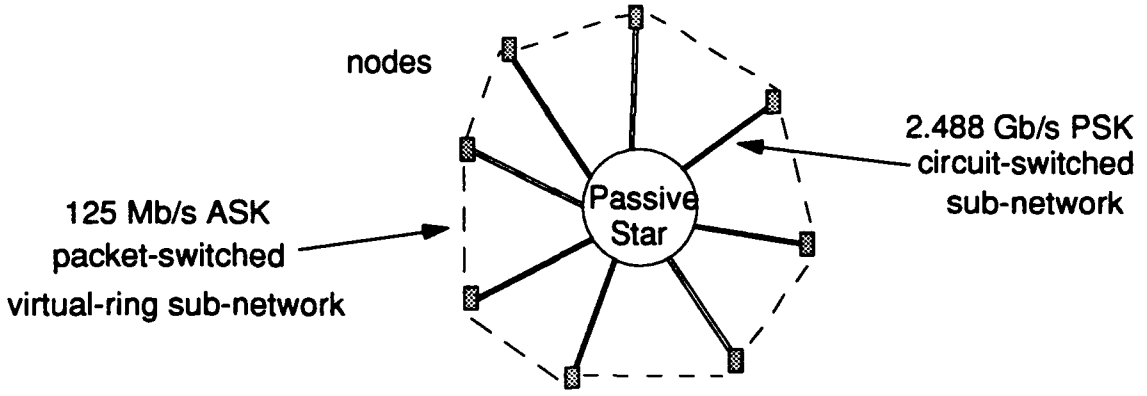

Figure 1: STARNET logical topology.

The packet-switched sub-network can be used for control of the high-speed sub-network and relative frequency stabilization of the WDM network, in addition to carrying payload packets. The two logical sub-networks are implemented with only one transmitter laser per node by multiplexing packet-switched data using amplitude-shift keyed (ASK) modulation and circuit-switched data using phase-shift keyed (PSK) modulation on the same optical carrier. Each node is equipped with two receivers to recover the ASK and PSK data separately. This new network architecture is novel and important because it addresses two fundamental problems with WDM networks: (1) the need to support both packet-switched and circuit-switched services, and (2) the need to control high-speed circuit connections *before* virtual circuits are set up.

To investigate simultaneous transmission and reception of ASK packet-switched and PSK circuit-switched data using the same optical carrier, we analyzed the impact of the amplitude modulation depth of the sensitivity of ASK and PSK receivers. An example of our results is shown in Figure 2. In this case, high-speed data are transferred via PSK modulation while low-speed data are transferred via ASK modulation. The sensitivity of the ASK receiver improves as the modulation depth is increased while the sensitivity of the PSK receiver deteriorates due to the reduced signal power at the PSK receiver when an ASK '0' is transmitted. For a modulation depth around 0.5, the ASK and PSK receivers operate with equal sensitivities. This point represents the optimum modulation depth for a node transceiver.

Figure 3 illustrates the opposite case when the high-speed data are transferred via ASK modulation and the low-speed data are transferred via PSK modulation. Comparison of Figure 3 with Figure 2 shows that the proper modulation format for the high-speed data is PSK and the

proper modulation format for the low-speed data is ASK. In Figure 3, there is no practical amplitude modulation depth where the ASK and PSK receiver sensitivities are equal.

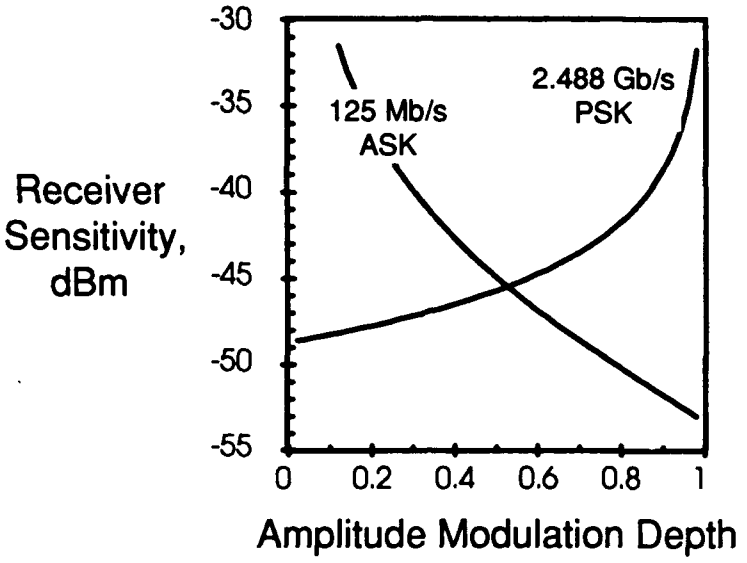

Figure 2: Theoretical ASK and PSK receiver sensitivity versus amplitude modulation depth.

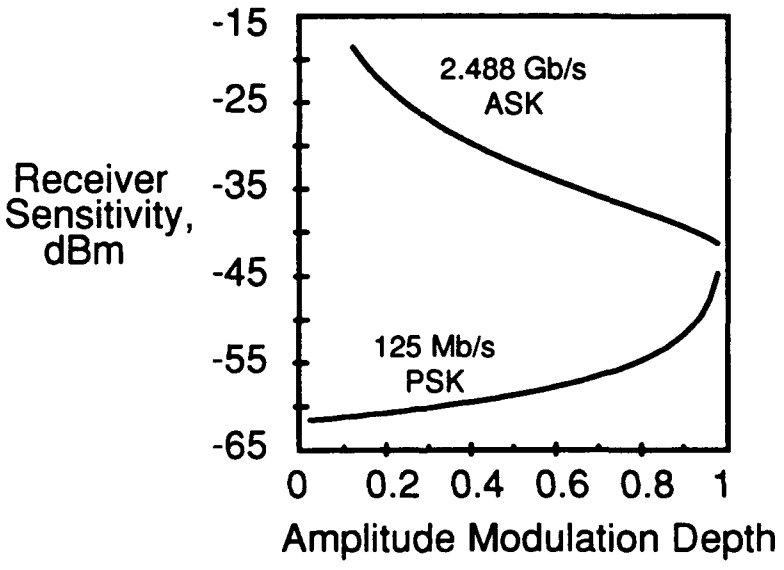

Figure 3: Theoretical ASK and PSK receiver sensitivity versus amplitude modulation depth.

To verify our theory experimentally, we constructed a complete experimental node transceiver. The transmitter has an output power of 5 dBm at 1.32 μm. The sensitivity of the

2.488 Gb/s PSK receiver is -33.3 dBm for a 2^7-1 pseudo-random bit stream (PRBS). The sensitivity of the 125 Mb/s ASK receiver is -45 dBm. With both amplitude and phase modulation on the same lightwave, the ASK and PSK receivers operate with equal sensitivities of -25 dBm for an amplitude modulation depth of 0.6. The resulting system power budget is 30 dB. This power budget is enough for a 100 node, 10 km diameter network.

High-speed optics-to-computer interface design: We have investigated the issue of WDM network-to-computer interface and designed a high-speed STARNET optics-to-computer interface for a RISC workstation. The workstation connects to a STARNET transceiver via electronic hardware modules which are installed in the DECstation's TURBOchannel™ I/O bus.

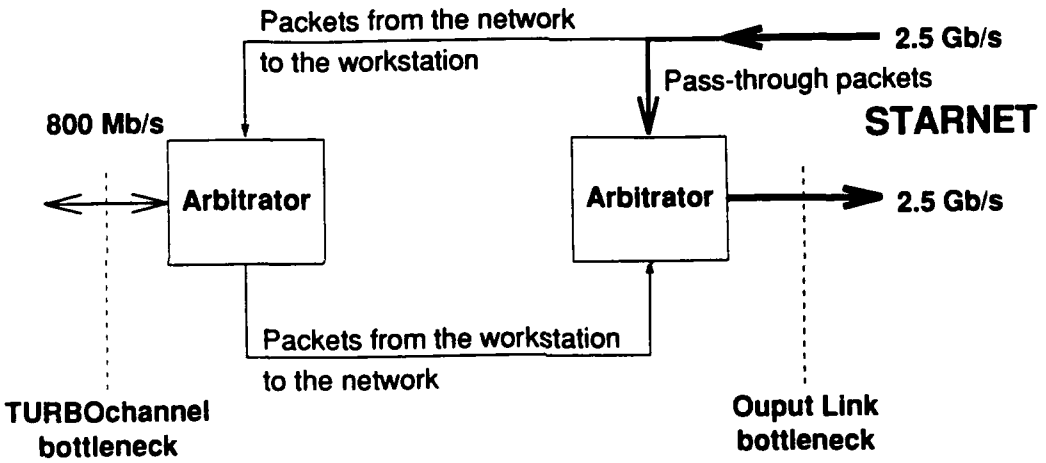

Figure 4: High-speed network bottlenecks.

The experimental STARNET transceiver provides full-duplex communication at a sustained rate of 2.488 Gb/s. A conservative estimate of the TURBOchannel I/O bandwidth available to the high-speed sub-network is 200-250 Mb/s (Fig. 4). Therefore, the STARNET transceiver is capable of sending and receiving at a rate 10 times greater than any current workstation bus can sustain. To take advantage of the remaining bandwidth of the STARNET transceiver, the high speed circuit switched sub-network interface is designed for multihop packet switching. Routing of incoming packets on the circuit-switched sub-network is done on-the-fly on a packet by packet basis. The headers of incoming packets are checked. If they are destined for the receiving node, they are placed in a receive FIFO. Packets not destined for the

workstation are forwarded to the node's output link without being seen by the node's local bus. The result is a high-speed 2x2 multihop packet switch architecture over the circuit-switched sub-network (Fig. 5).

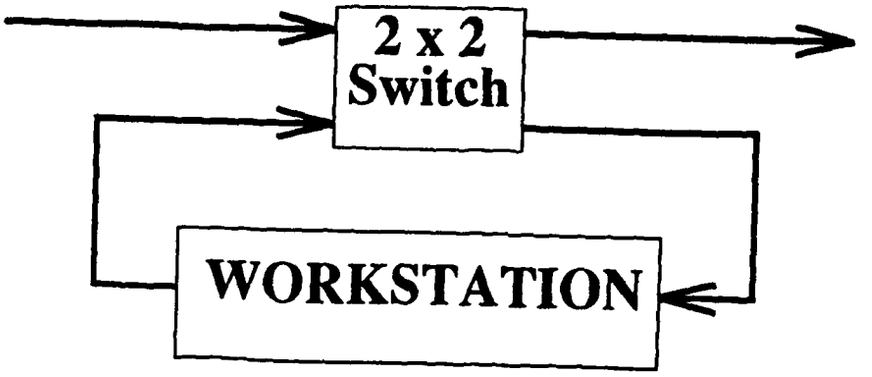

Figure 5: The high speed interface will act like a 2x2 switch..

2. Coherent Analog Links

Angle-Modulated Systems: In the previous ONR Status Report, we described our findings that coherent FM links are highly sensitive to laser phase noise. Given the wide linewidths of present semiconductor DFB lasers, these links cannot attain a higher dynamic range than AM direct-detection links unless phase noise is canceled using a dedicated circuit. To address this problem, we have investigated two primary methods of phase noise cancellation in angle-modulated systems: embedded reference and interferometric links. We performed theoretical analysis of these systems to investigate to what extent they are successful in suppressing phase noise. Our results indicate that the embedded reference technique, known to be effective in phase-modulated CATV systems utilizing subcarrier multiplexing, exhibits inadequate phase noise suppression for wideband high dynamic range applications. Angle-modulated interferometric systems can achieve complete phase noise suppression if the path lengths of the interferometer are well-matched. However, such a configuration requires the use of external modulation.

Since interferometric links have the potential to surpass the dynamic range performance of AM direct-detection links, we focused on similar links in our studies.

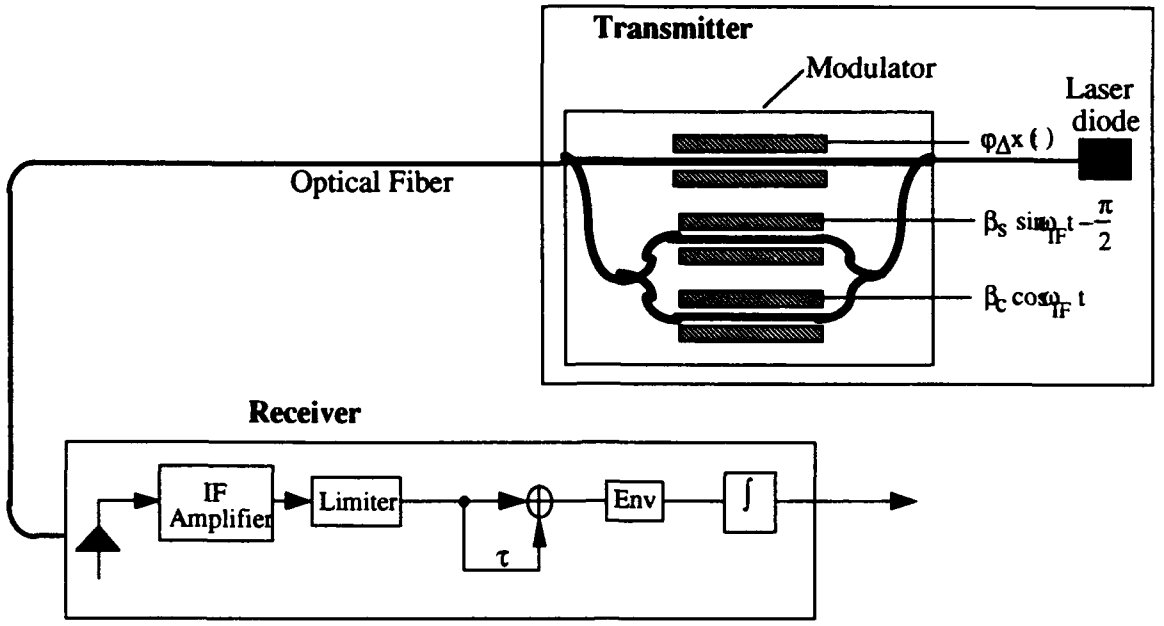

Figure 6: Block diagram of the heterodyne interferometric PM link.

We have proposed and analyzed a heterodyne interferometric PM link (HIPM) (Figure 6) which utilizes a novel external phase modulator to cancel the phase noise of the transmitter via mixing at the photodiode. The outputs of the modulator are also frequency-shifted to an intermediate frequency (IF) at the photodiode, converting what appears to be a homodyne link to a heterodyne link. Transmitter relative-intensity noise (RIN) is suppressed if the intermediate frequency is chosen to be much larger than the laser relaxation resonance frequency.

The transmitter consists of a CW laser and a novel three-leg modulator. One leg of the modulator is driven by the signal. The other two legs are driven by quadrature CW RF signals at a frequency ω_{IF}, optically phase shifted by $\pi/2$ from each other. After traversing a fiber-optic link, the signal is detected at the receiver. The optical signals of the second and third legs of the modulator mix with the signal at the detector and result in a series of single-sideband signals at multiples of ω_{IF}. The second and third legs are thus roughly equivalent to a single-sideband frequency shifter. Following the photodiode, the signal is amplified and limited. It is then put through a delay-line filter, an envelope detector, and an integrator; these three components function in tandem as a phase demodulator.

We have analyzed the nonlinearities generated in the HIPM link by the sinusoidal delay-line filter characteristic and found the limit of the dynamic range. The spurious-free dynamic range (SFDR) of the HIPM-based link is equal to the signal-to-noise ratio (SNR) at the optimum phase modulation depth. Figure 7 shows the worst-case SFDR of an HIPM link and that of a standard AM link for a 1 to 2 GHz signal band (f_{min} to f_{max}). The two cases considered

correspond a high RIN semiconductor laser (RIN = -130 dB/Hz) and a low RIN semiconductor laser (RIN = -155 dB/Hz). In both cases, we take the laser relaxation resonance frequency to be 2 GHz. The HIPM link shows an SFDR advantage of 3 dB over an AM DD link for small signal power values where the impact of RIN is insignificant. This advantage increases at higher powers where the AM DD noise is dominated by RIN. At an optical power level of 10 mW with the low RIN laser the SFDR of the HIPM link is 7 dB larger than that of the AM DD link. For the high RIN laser, this advantage increases to 22 dB. The improvement in SFDR over the AM link generated by the HIPM link becomes larger as the IF is increased due to both the reduced nonlinearity of the HIPM link and to its suppression of RIN. The HIPM link provides the greatest advantage for high power, high RIN sources.

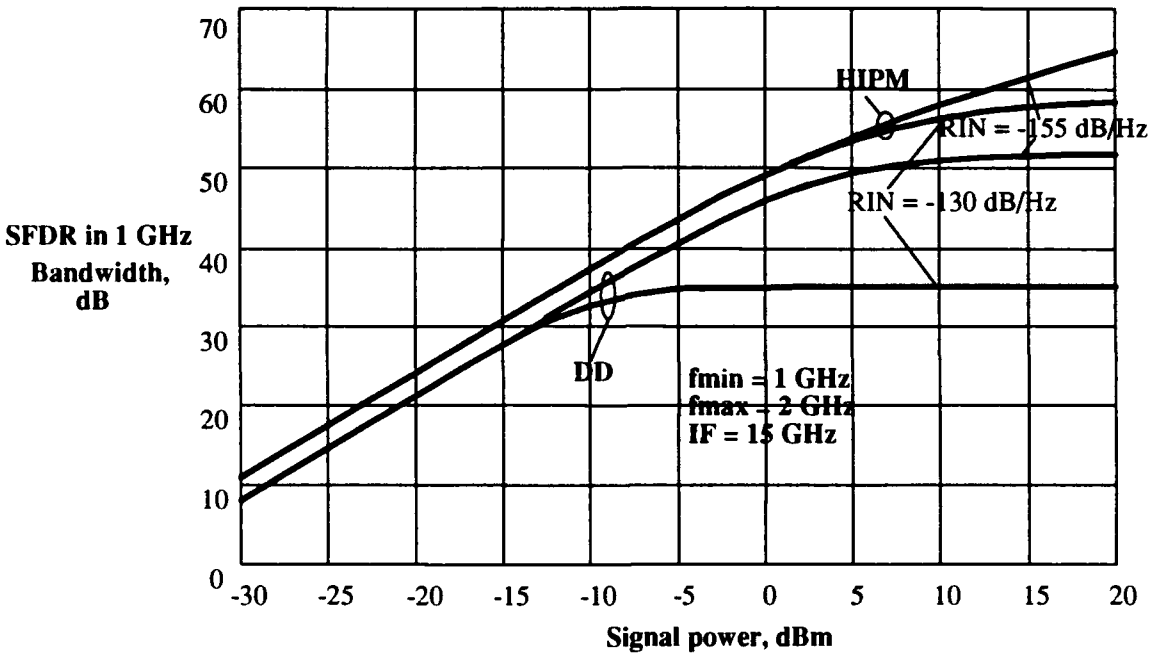

Figure 7: Spurious free dynamic range versus signal power.

Amplitude-modulated systems: We continued our theoretical investigations of linewidth-insensitive coherent optical analog systems. A block diagram of the coherent AM analog link[1] is shown in Figure 8. For that link, we analyzed the optimum IF filter bandwidth, the fundamental limit of the dynamic range (FLDR), and the spurious-free dynamic range (SFDR). The system noises considered in these analyses are laser phase noise, shot noise, thermal noise, and laser relative intensity noise (RIN). We also analyzed the impact of device nonlinearities on the system performance.

[1] *This link is being experimentally investigated in our laboratory under Air Force grant number F30602-91-0141*

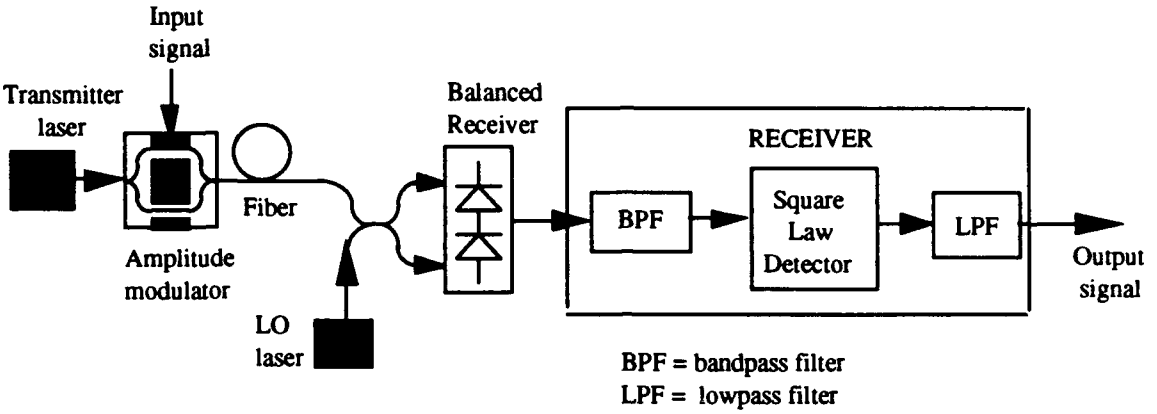

Figure 8: Block diagram of the coherent AM analog optical link.

The output current of the photodetector is processed by the bandpass filter, the square law detector and by a low pass filter. The performance of the system depends on the bandwidths of the bandpass filter and lowpass filter. A narrow bandpass filter (with respect to the signal bandwidth) would cause some of the signal power to be lost thereby resulting in phase noise-to-amplitude noise conversion. On the other hand, a wide bandpass filter would collect more additive noise. We evaluated the optimum IF bandwidth and found it to be given by:

$$B_{BPF,OPT} \approx \sqrt{\frac{2 \cdot \Delta\nu \cdot m^2 \cdot A^4}{\pi \cdot \eta^2 \cdot B_{LPF}} + (2 \cdot B_{LPF})^2} \tag{1}$$

where $\Delta\nu$ is the IF linewidth, m is the modulation depth, A is the IF signal amplitude, η is the noise power spectral density, and B_{LPF} is the lowpass filter bandwidth (which is equal to the signal bandwidth).

The dynamic range is defined as the ratio of the maximum allowable RF input power to the minimum required RF input power. The fundamental limit of the dynamic range (FLDR) is obtained by assuming no nonlinearities and a single-tone signal with modulation index of one. We showed that for large optical powers, the FLDR can be approximated by:

$$FLDR \approx \Gamma_\phi \cdot \frac{A^2}{4 \cdot \eta \cdot B_{LPF}} \tag{2}$$

where

$$\Gamma_\phi \equiv \frac{4}{\pi} \cdot \tan^{-1}\left(\frac{2 \cdot B_{BPF}}{\Delta\nu}\right) + \frac{2}{\pi} \cdot \tan^{-1}\left(\frac{2 \cdot B_{BPF}}{\Delta\nu}\right) - 2. \tag{3}$$

Γ_ϕ represents the reduction in dynamic range due to phase-to-intensity noise conversion and is independent of optical power. One important conclusion from expression (2) is that the degradation due to the laser linewidth can be made negligible by optimizing the bandbass filter bandwidth.

When the maximum allowable signal power is determined by the intermodulation distortions, the dynamic range is known as the spurious-free dynamic range (SFDR). We showed that when the external modulator is the dominant source of distortion, the SFDR can be approximated by:

$$SFDR \approx 4 \cdot \Gamma_\phi^{2/3} \cdot \left[\frac{4 \cdot A^4}{16 \cdot A^2 \cdot \eta \cdot B_{BPF} + 4 \cdot \eta^2 \cdot B_{BPF} \cdot (4 \cdot B_{BPF} - B_{LPF})} \right]^{2/3} \quad (4)$$

We have investigated the impact of the following imperfections on the dynamic range: modulator nonlinearity, laser RIN and laser linewidth. We discovered that system nonlinearities are the dominant effect and reduce the dynamic range by 12-18 dB. The SFDR can be improved by employing a more linear modulator or by utilizing linearization techniques. For optical systems using low RIN semiconductor lasers (RIN < -160 dB/Hz), RIN reduces the dynamic range by a factor of 3 (for optical powers < 5 mW). Most importantly, with proper system design, the coherent link is essentially linewidth-insensitive.

Our next step in the coherent AM portion of the project is to analyze the noise figure and RF power transfer ratio of the coherent AM analog optical link. This will allow us to improve the understanding of the interrelationship between the system and device parameters.

Directly Modulated FM-SCM Systems with an Optical Discriminator: We have collaborated with GTE Labs on this combined theoretical and experimental effort. The primary work done at Stanford has been the theoretical analysis of frequency modulated-subcarrier multiplexed (FM-SCM) systems using the Carson-Fry approach. In addition, a parallel method for system optimization using the Fourier-Bessel expansion of the frequency spectrum of FM signals has been developed.

The system shown in Figure 9 uses direct frequency modulation of a distributed feedback (DFB) laser and a fiber Fabry-Perot (FFP) interferometer for optical frequency discrimination. After the photodetector and amplification, a down-converter and FSK demodulator extract the desired video signals. The measured carrier-to-noise ratio (CNR) at the photodiode must be approximately 17 dB to give a bit error rate (BER) of 10^{-9} at the output. Direct frequency modulation is a linear modulation format for small modulation indices, which must be used to

prevent mode-hopping. However, to obtain contributions from both the frequency modulation and the simultaneous spurious amplitude modulation components, a FFP must be used before the photodetector. The novel analysis chooses the FFP operating point and modulation index which optimize system performance.

The effects taken into account in our investigations include thermal noise, the phase shift between the spurious AM signal generated during direct frequency modulation and the FM signal, and the nonlinear FM-to-AM conversion by the FFP. The conversion of laser linewidth to relative intensity noise (RIN) is ignored because thermal noise is dominant in this system even for the wide linewidths of semiconductor lasers.

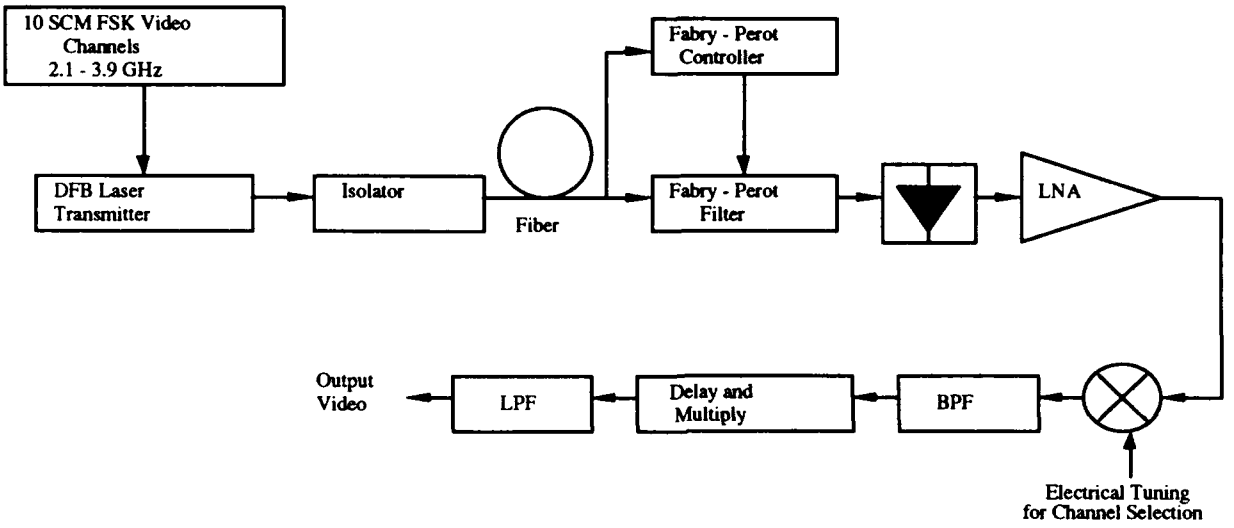

Figure 9: Block diagram of FM-SCM system.

Figure 10 shows the carrier-to-noise ratio versus the FM modulation index obtained using two different theoretical methods. The Bessel method is exact but rapidly becomes computationally unmanageable for large numbers of channels. Even for ten channels, the method is useful only for low FM modulation indices. This restriction is not severe, however, since it is only possible at present to use low modulation indices when directly frequency modulating DFB lasers with wideband (on the order of 1 GHz) signals.

In the Carson-Fry method, the solution is not uniformly convergent, but rather is asymptotic. This means that the solution will converge to within a finite interval of the true value before diverging. Even so, for low FM modulation indices, the CNR predictions of the Carson-Fry method for this system agree very closely with the results obtained from the Bessel method, as shown in Figure 10. We have developed precise criteria for the regions of applicability for this method. The general requirement is that the signal frequency deviations about the carrier be much less than the 3 dB bandwidth of the FFP. When the Carson-Fry model

is applicable, it is much less computationally expensive than the Bessel method, particularly if there are more than ten channels.

Experimental measurements of CNR made for the three operating points shown in the figure (T = 0.25, 0.5, and 0.75 on the positive-slope side of the FFP transfer function) for FM modulation indices between 0.05 and 0.6 all are within 1 dB of the theoretical predictions. At an index of 0.5 and an operating point of 0.75, a CNR at the photodiode of 23 dB is obtained. Assuming low-noise amplification, this is sufficient for transmission of FSK video.

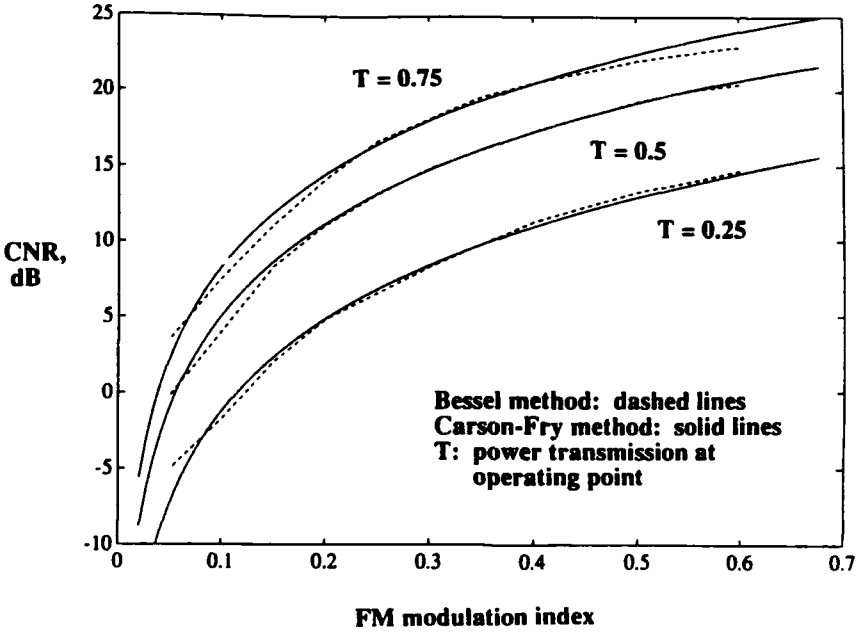

Figure 10: Carrier-to-noise ratio versus FM modulation index.

3. Fiber Nonlinearities

Four-Wave Mixing: We evaluated the performance of optical WDM systems in the presence of four-wave mixing (FWM) via both theoretical analysis and simulations. The nonlinear FWM process limits the maximum optical power that can be launched into fibers, and the shot noise limits the minimum required power at the receiver. We have evaluated the power budget defined as the ratio of the maximum transmitter power to the minimum optical power at the receiver, and derived the maximum transmission distance.

In the theoretical analysis, we used Gaussian approximation to model the FWM interference. To investigate the validity of this approximation, we performed computer simulations for 16-channel WDM ASK systems. The 16 independent optical channels were computer-generated with random laser phase noise, uncorrelated random data streams, and independent clocks with random jitter. The simulation was carried out for both NRZ and

Manchester-coded cases. Using 16 optical channels, the IF signal was generated by the simulation program. Next, the program evaluated the probability density function (pdf) of FWM-impaired signals at the envelope detector output. Finally, the receiver BER was evaluated for NRZ and Manchester codes using the simulated pdf's of FWM-impaired signals.

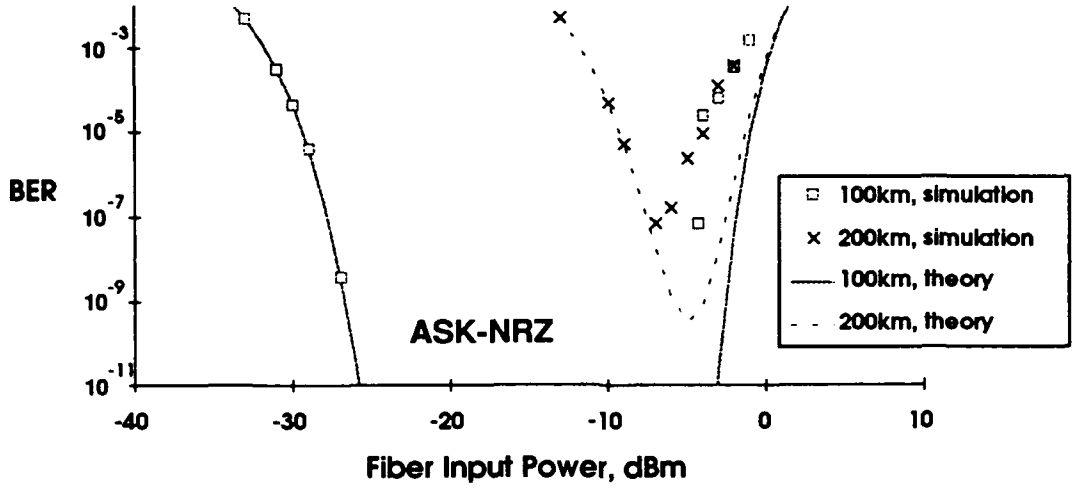

(a) ASK system with NRZ coding

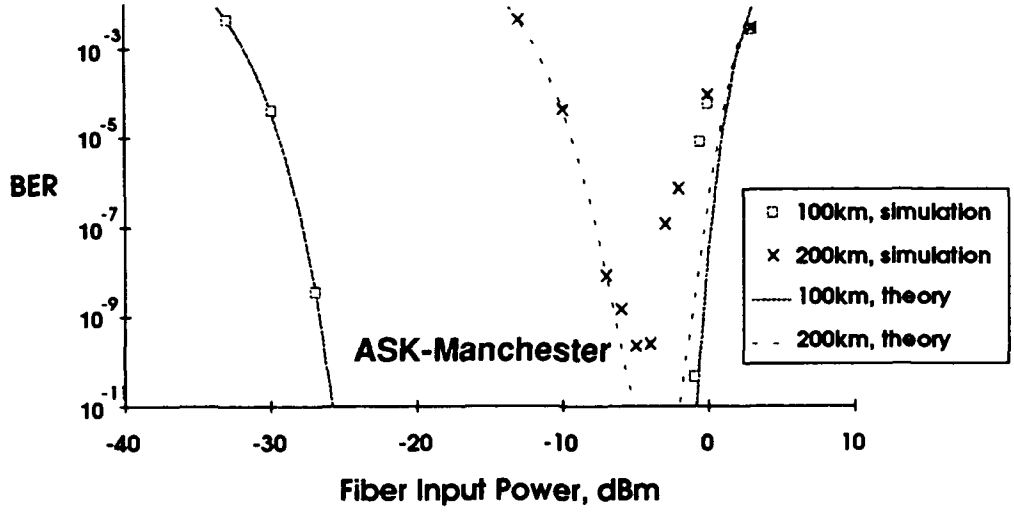

(b) ASK system with Manchester coding

Figure 11: Bit error rate of 16-channel ASK systems impaired by FWM.

The simulation and theoretical BER results are shown in Figures 11a and 11b for NRZ and Manchester coding, respectively. The BER curves in Figure 11 are shown for the 8th

channel (the worst case) of the 16-channel WDM system using a dispersion shifted (DS) fiber versus optical input power to the fibers with 100 km and 200 km lengths. The rest of system parameters are as follows: n = 1.47, λ = 1.55 μm, α = 0.2 dB/Km, channel spacing = 10 GHz, bit rate = 1 Gbit/s, laser linewidth = 10 MHz, effective core area A_{eff} = 55 μm^2, third-order nonlinear susceptibility $\chi_{1111} = 6x10^{-15}$ cm^3/erg, photodiode responsivity R = 0.6 amp/watt and group velocity dispersion = 15 ps/km·nm for non-DS (NDS) and 0.5 ps/km·nm for DS fibers.

It is evident that in the low power region the BER is limited by shot noise, while in the high power region the BER is determined by FWM. There is an optimum input power level yielding the minimum BER. This minimum value of BER increases with increase in fiber length. The maximum transmission distance for a BER $\leq 10^{-9}$ is 211 km for a Manchester coded system using the DS fiber; this distance is about 9 km longer than that for the NRZ system.

Further inspection reveals that the theoretical results are similar to the simulation results but overestimate the receiver sensitivity especially near the threshold input power levels where the FWM interference becomes dominant over shot noise. The discrepancy is caused by the Gaussian model of the FWM interference used in the theoretical analysis .

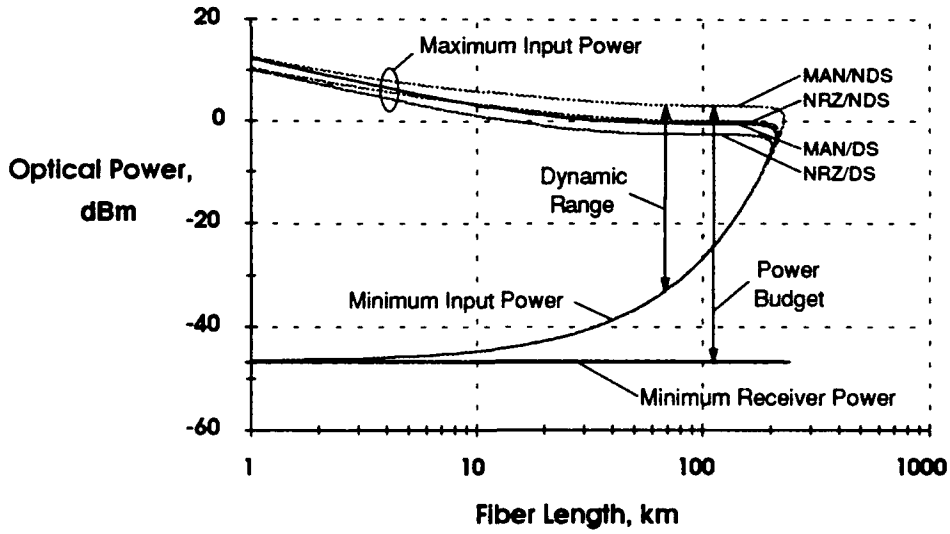

Figure 12: Maximum transmission distance of NRZ and Manchester coded ASK systems impaired by FWM.

The maximum and minimum input powers for the 8th channel of a 16 channel WDM system needed to maintain BER below 10^{-9} are shown in Figure 12. The ratio of the maximum power to the minimum power is defined as the dynamic range. Manchester coded ASK systems have about 2 dB larger dynamic range than the corresponding NRZ coded ASK systems. The

system power budget is defined as the ratio of the maximum input power to the minimum receiver power needed to keep BER below 10^{-9}. Figure 12 shows that the power budget decreases at long fiber lengths due to the drop of the maximum allowable input power caused by FWM. Manchester coded systems show about 2 dB improvement with respect to NRZ systems; the power budget of the systems using NDS fiber is 3 dB larger than that of the systems using DS fiber.

Table I summarizes the maximum transmission distances for coherent communication systems with ASK and DPSK modulation formats, NRZ and Manchester codings, as well as DS and NDS fibers.

Table I

Maximum transmission distances.

Fiber Type \ Modulaton Format / Coding		ASK	DPSK
DS	NRZ	202 km	221 km
	MAN	211 km	233 km
NDS	NRZ	216 km	244 km
	MAN	227 km	274 km

Inspection of Table I reveals that the worst case transmission distance is 202 km for DS fiber, NRZ coding, and ASK modulation and the best case transmission distance is 274 km for NDS fiber, Manchester coding, and DPSK modulation.

Fiber-Induced Parasitic Phase Modulation: In the previous report period, we experimentally observed thermal acoustic vibrations in the fiber and the resulting parasitic phase modulation. In this period, based on these experimental observations, we performed a theoretical analysis of the impact of parasitic fiber-induced phase modulation on ultra-long distance DPSK optical communication systems.

Our results show that the performance of ultra-long distance optical DPSK system can be impaired by thermal acoustic modulation. Figure 13 shows the calculated bit error rate of 1 Gb/s DPSK systems versus received optical power for different fiber lengths in the presence of fiber

induced phase noise, laser phase noise, and shot noise. The total laser linewidth is 6 MHz. Inspection of Figure 13 reveals that the power penalty at the BER of 10^{-9} is 2.7 dB for the finite laser linewidth. The power penalties for the fiber induced phase noise are 0.2 dB, 0.5 dB, 1.5 dB, and 3.9 dB for transmission distances of 1000 km, 2000 km, 5000 km, and 10000 km respectively.

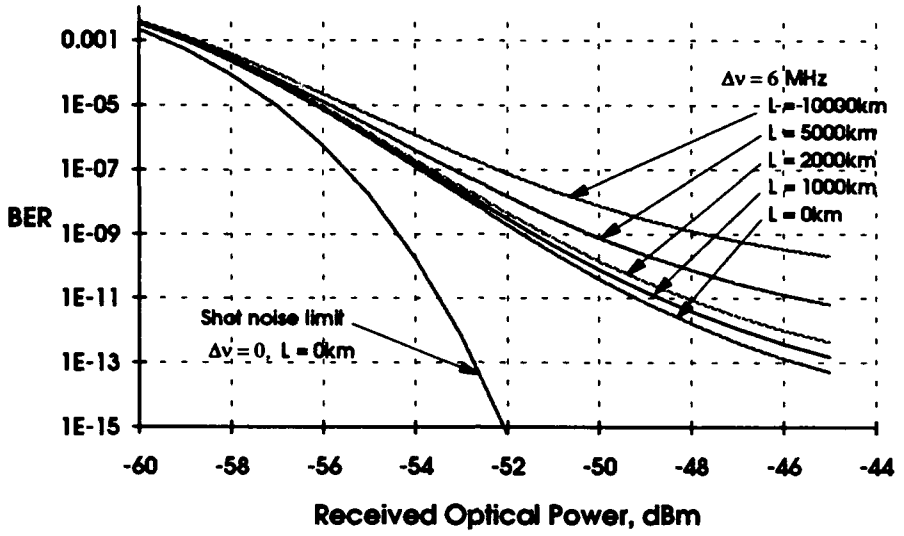

Figure 13: Calculated bit error rate of 1 Gb/s DPSK heterodyne systems

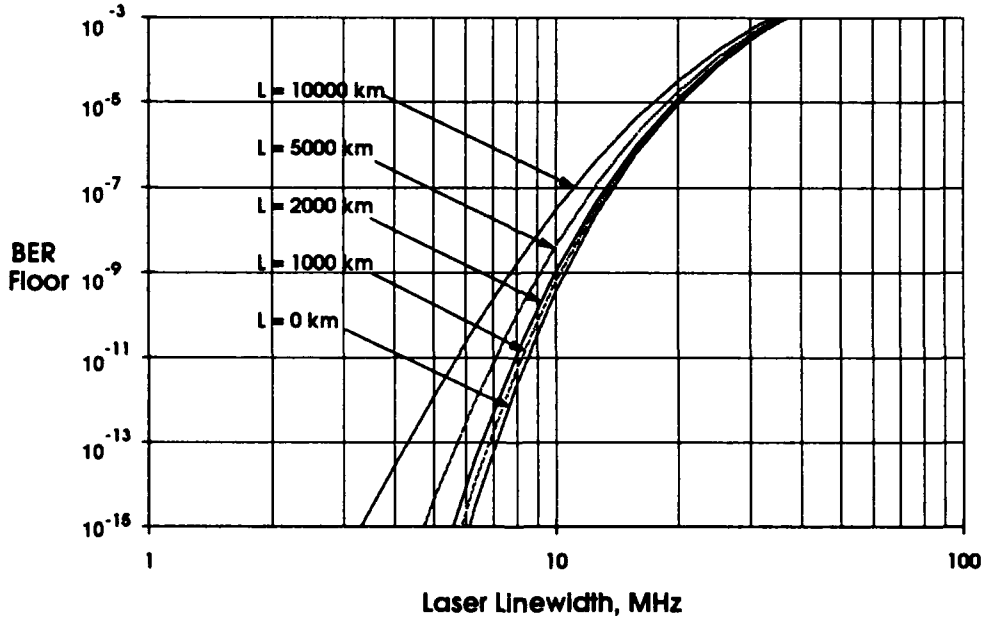

Figure 14: Calculated BER floor of 1 Gb/s DPSK heterodyne systems.

Figure 14 shows the calculated BER floor of 1 Gb/s DPSK systems versus laser linewidth for different fiber lengths in the presence of thermal acoustic phase noise. Shot noise is ignored to show the BER floor which is the minimum BER that can be achieved at high received power. Figure 14 reveals that the BER floor increases as the transmission distance increases. At transmission distance greater than 2000 km, the fiber induced phase noise deteriorates system performance significantly. On the other hand, when transmission distance is less than 1000 km, the BER floor is less than two times the BER floor of back-to-back system. Therefore, the fiber induced phase noise is negligible in DPSK systems with transmission distances less than 1000 km.

Solitons: We have theoretically investigated the possibility of controlling the speed of three-wave envelope solitons in an optical fiber. Three-wave envelope solitons (TWES) are three waves (one acoustic and two optical) that propagate together as one. The envelope of the acoustic wave and one optical wave are bright pulses with their maxima at the center of the TWES. The second optical wave is a dark pulse at the center of TWES.

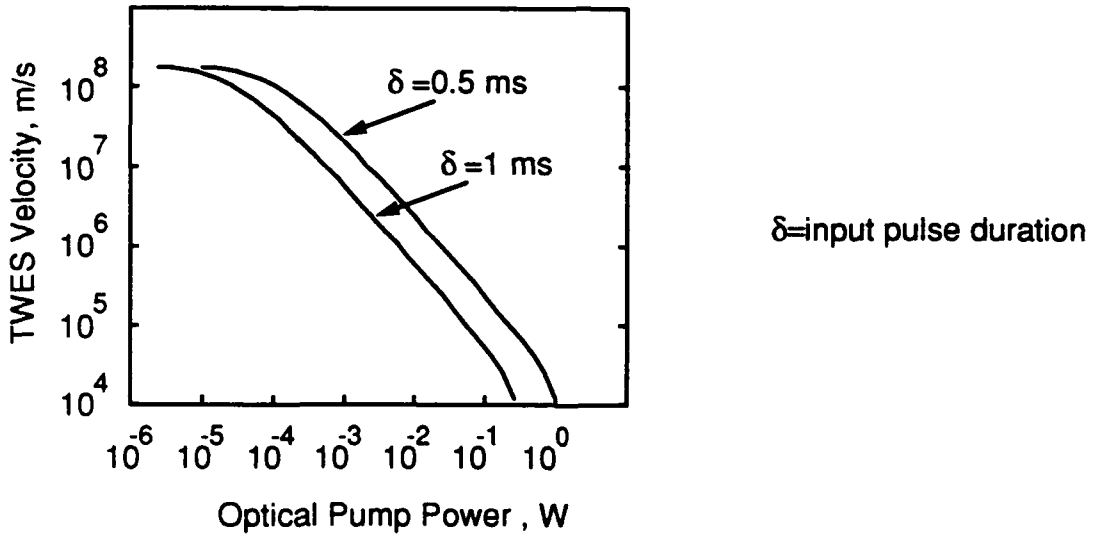

Figure 15: Three-wave envelope soliton velocity versus optical pump power.

To generate a TWES, two optical co-propagating waves must be synchronously modulated and launched into the fiber. The acoustic wave is generated by nonlinear coupling with intermodal beating in a dual mode fiber. The second order nonlinearity responsible for this process is the same nonlinearity leading to stimulated forward Brillouin scattering. The introduction of a π phase shift in the incident Stokes beam is required for generating TWES. The duration of TWES is determined by the shortest of the following: the duration of injected

pulses, the nonlinear time, and the attenuation time. Hence, if the injected pulse duration (δ) is greater than either the nonlinear time or the attenuation time then the TWES duration is determined by the fiber. If the injected pulse duration time is smaller than both the nonlinear time and the attenuation time, then the TWES duration is controlled by external modulation.

The TWES velocity is controlled by the pump power. For dual-mode fibers, it can be adjusted between 2×10^8 m/s (the speed of "regular" light in the fiber) and 2×10^4 m/s (twice the speed of a linear acoustic wave in the fiber) by adjusting the pump power between 0.01 and 200 mW. This dependence is illustrated in Figure 15.

OPTICAL COMMUNICATIONS RESEARCH LABORATORY. ONR PROJECT
JOURNAL AND CONFERENCE PAPERS SUBMITTED, ACCEPTED or PUBLISHED BETWEEN SEPTEMBER 1, 1992, AND FEBRUARY 28, 1993.

PAPER NO.	TITLE	AUTHORS	STATUS	JOURNAL OR CONFERENCE NAME
1	Performance Optimization of Directly Modulated FM-SCM Systems with Optical Discriminator	G. Fiksman, R. Gross, J. Fan, L. G. Kazovsky	Submitted on 12/20/92	IEEE Photonics Technology Letters
2	Impact of Finite Frequency Deviation on the Performance of Dual-filter Heterodyne FSK Lightwave Systems	O.K. Tonguz, M.O. Tanrikulu, L.G. Kazovsky	Published on 2/1/93	IEEE/OSA Journal of Lightwave Technolog
3	Space Division Switches Based on Semiconductor Optical Amplifiers	R.F. Kalman, L.G. Kazovsky, J.W. Goodman	Published on 10/1/92	IEEE Photonics Technology Letters
4	Linewidth -Insensitive Coherent Analog Optical Link Using Semiconductor Lasers	T. K. Fong, J. Sabido, L. G. Kazovsky	Accepted on 1/28/93	IEEE Photonics Technology Letters
5	Experimental PSK/ASK Transceiver for the STARNET WDM Computer Communication Network	M. Hickey, C. Barry, C. Noronha, L. G. Kazovsky	Accepted on 1/28/93	IEEE Photonics Technology Letters
6	STARNET: a Multi-Gbit/s Optical LAN Utilizing a Passive WDM Star	L. G. Kazovsky, P. T. Poggiolini	Will be published on 5/1/93	IEEE/OSA Journal of Lightwave Technolog (Special Issue)
7	Three-Wave Envelope Solitons: Possibility of Controlling the Speed of Light in the Fiber	N. L. Taranenko, L. G. Kazovsky, Y. N. Taranenko	Will be presented on 8/1/93	URSI General Assembly, Kyoto, Japan
8	A Novel Phase-Modulated Analog Optical Link	R. F. Kalman, J. C. Fan, L. G. Kazovsky	Submitted on 12/14/92	SPIE's Intl. Symposium OE/Fibers '93, San Diego, CA
9	Theoretical and Exceptional Investigations of the Dynamic Range of High Frequency Coherent AM Optical Links Using Semiconductor Lasers	J. Sabido, M. Tabara, T. K. Fong, C. L. Lu, L. G. Kazovsky	Submitted on 12/14/92	SPIE's Intl. Symposium OE/Fibers '93, San Diego, CA
10	A Multi-Gbit/s Optical LAN Utilizing a Passive WDM Star: Towards an Experimental Prototype	L. G. Kazovsky, C. Barry, M. Hickey, C. Noronha, P. T. Poggiolini	Presented on 3/1/93	IEEE INFOCOM, San Francisco, CA
11	An Experimental PSK/ASK Transceiver for a multi-Gb/s WDM Network	M. Hickey, C. Barry, C. Noronha and L. Kazovksy	Presented on 2/24/93	OFC '93, San Jose, CA
12	Scattering from Guided Acoustic Waves in Optical Fiber and It's Influence on DPSK Optical Communication Systems	T. K. Chiang, L. G. Kazovsky	Presented on 2/22/93	OFC '93, San Jose, CA
13	Optimization of Directly Modulated FM-SCM Systems Using an Optical Frequency Discriminator	G. Fiksman, R. Gross, J. C. Fan, L. G. Kazovsky	Presented on 2/22/93	OFC '93, San Jose, CA
14	Supression of Four-Wave Mixing Crosstalk in WDM Systems Using Manchester Coding and DPSK Modulation	H. Lee, L. G. Kazovsky	Presented on 2/22/93	OFC '93, San Jose, CA

PAPER NO.	TITLE	AUTHORS	STATUS	JOURNAL OR CONFERENCE NAME
15	Binary and Multilevel Polarization Modulation: Experimental System Design	S. Benedetto, L. G. Kazovsky, P. T. Poggiolini, C. A. Barry, A. Djupsjobacka, B. Lagerstrom, S. Chandrasekhar, U. Koren	Presented on 9/30/92	SPIE's Intl. Symposium OE/Fibers '92, Multigigabit Fiber Communications, Boston, MA
16	Combined ASK/PSK Modulation Format for the STARNET Wavelength Division Multipexed Local Area Network	M. Hickey, L. G. Kazovsky	Presented on 9/30/92	SPIE's Intl. Symposium OE/Fibers '92, Multigigabit Fiber Communications, Boston, MA
17	Coherent Optical Communications (Short course)	L. G. Kazovsky	Presented on 9/30/92	SPIE's Intl. Symposium OE/Fibers '92, Multigigabit Fiber Communications, Boston, MA
18	Starnet-E: A Broadband Wavelength Division Multiplexed Optical Local Area Network	L. G. Kazovsky, C. F. Barry, C. A. Noronha, P. T. Poggiolini	Presented on 9/30/92	SPIE's Intl. Symposium OE/Fibers '92, Multigigabit Fiber Communications, Boston, MA
19	Multigigabit Optical Networking (Tutorial overview)	L. G. Kazovsky, K. Liu, C. A. Noronha	Presented on 9/30/92	SPIE's Intl. Symposium OE/Fibers '92, Multigigabit Fiber Communications, Boston, MA
20	Impact of Four Wave Mixing on Manchester Coded Optical WDM Communication Systems	H. Lee, L. G. Kazovsky	Presented on 9/30/92	SPIE's Intl. Symposium OE/Fibers '92, Multigigabit Fiber Communications, Boston, MA